Soft Matter

View Online
Dynamic Article Links

Cite this: *Soft Matter*, 2011, **7**, 2042

www.rsc.org/softmatter

PAPER

Red blood cell dynamics: from spontaneous fluctuations to non-linear response

Young Zoon Yoon,[ab] Jurij Kotar,[a] Aidan T. Brown[a] and Pietro Cicuta*[a]

Received 6th October 2010, Accepted 2nd December 2010
DOI: 10.1039/c0sm01117g

We studied experimentally the mechanical properties of the red blood cell. By attaching beads biochemically on the cell membrane at diametrically opposite positions, the membrane movements can be detected very accurately, and a deformation of the cell can be imposed. A measurement of the mechanical properties at very small amplitudes is obtained by fluctuation analysis, and compared to the stiffness at larger deformations, obtained by stretching the cells *via* optical traps whilst monitoring the force. The cells are also probed at various conditions of pre-strain. These measurements show clearly a stiffening with strain and with pre-strain, which is strongest at low frequencies of deformation. The cell is measured to be slightly softer from fluctuation analysis, but consistent simply with the fact that the oscillation amplitude in fluctuations is very small. There is no evidence in these experiments of non-thermal sources of membrane motion, although non-thermal noise may be present within experimental error.

1 Introduction

From the mechanical point of view, biological cells are very complex materials with highly unusual dynamical response properties: they usually exhibit viscoelasticity and are often non-linear, as well as displaying non-thermal active responses.[1] These properties stem from the architecture of the cytoskeleton: a network of semiflexible protein filaments, crosslinked by both passive and active (motors) protein groups. The result is an effective stiffness which depends sensitively on the applied stress, deformation protocol and environmental conditions.[2] The filaments present in most cell types are F-actin, intermediate filaments and microtubules: generally they confer rigidity to cells, and to tissues at larger scales.[3,4] The red blood cell (RBC, or erythrocyte) is a biological structure of relative simplicity and exceptional softness. It can be broadly described as a bilayer membrane, coupled to a thin and tenuous cortical cytoskeleton composed of spectrin filaments (in most mammals).[3] Coupling is maintained *via* complexes of a few different proteins (ankyrin, band 3 and band 4.1). In mammals, the red blood cells lack a nucleus and intra-membrane organelles.[5] The outer membrane, held under tension by the cortical cytoskeleton, encloses a dense solution of haemoglobin. Transport of oxygen is the key physiological role of this cell, and this is crucially linked to its ability to deform and flow through small spaces in the lungs and peripheral circulatory system. The mechanics of individual cells is strongly coupled to the rheology of whole blood.[6] Despite the simplicity of the cellular architecture and the high deformability, the mechanics of this cell shares some features of interest with more complex cells, including non-linearity[7] and possibly non-thermal dynamics.[8] The RBC has been and continues to serve as a useful model system to understand general aspects of cell mechanics.[9]

The response of cells to external stresses is a topic of current interest. Suspended cells have been shown to respond non trivially to applied forces.[10] Adherent cells tend to develop tension spontaneously on a substrate, and they respond to extracellular elasticity.[11,12] This implies effects at various systemic levels in the cell, from gene regulation up to the purely physical response of the cytoskeleton. Forces are a key factor in development.[13,14] Mechanical probing has been performed with different techniques on different types of eukaryotic cells, and in most cases tends to show a broad spectrum of relaxation times.[15,16] The simple architecture of the RBC is useful in this context, acting as a model in which the cytoskeleton and the membrane are the only structural elements that need to be considered. Another way to address the role of the cytoskeleton is to work with *in vitro* reconstituted systems. It has been shown that externally imposed forces (pre-stresses) influence strongly the mechanical properties of reconstituted cytoskeletal networks: the applied stress stiffens the cytoskeletal network, bringing the response into a non-linear regime.[17,18] Despite the importance of cell dynamics, the mechanical properties of the whole cell are less well understood than *in vitro* systems. There is still debate on the origin of nonlinearity in response to deformation.[19–22] For the "simple" RBC, while the question of cell shape[23] is relatively well understood, there are key open questions on the presence of non-thermal (ATP-driven) shape fluctuations (seen in ref. 8,24 but absent in ref. 25), and on how to include in a cell mechanical model the molecular changes induced in the cell by deformation.[5,26] Actin-coated vesicles have been studied both

[a]*Cavendish Laboratory and Nanoscience Center, University of Cambridge, JJ Thomson Avenue, CB3 0HE Cambridge, UK. E-mail: pc245@cam.ac.uk*
[b]*Department of Physics, Sungkyunkwan University, Suwon, 440-746, Korea*

experimentally[27,28] and theoretically[29] as architectural analogs of cells with a cortical cytoskeleton.

Microrheology is a general method by which the motion of microscopic tracer particles embedded in a material,[30] or the motion of components of the system itself,[31,32] is analysed obtaining mechanical and rheological properties of the material. Single particle microrheology has been applied also to spatially heterogeneous conditions, such as a bead attached to a membrane.[27,28] If pairs of beads are embedded in a homogeneous medium, then two-point microrheology, based on measuring the cross-correlated thermal motion of pairs of tracer particles, can be used to overcome some important limitations of single-particle microrheology: the dependence on the size or shape of the tracer particle, and the coupling between the tracer and the medium.[33] However in the case of particles attached to a single cell suspended in a liquid medium, as in ref. 10 and in the present work, extracting the cell mechanics is not so straightforward and the geometry of the system needs to be considered carefully, since forces can be transmitted both through the cell and through the surrounding liquid. The power of this technique is that two complementary measurements of the system's response are possible: by observing the intrinsic (thermal or otherwise) motion of the attached beads ("passive"), or by moving the beads and stretching the cell ("active"). If the cell has non-thermal sources of noise, there can be a key difference in the measured mechanical response between the active and passive experiments. The additional non-thermal noise would lead to an apparent softening of the material in the passive measurement. In recent work, this type of comparison of active and passive response functions has been used to highlight non-thermal processes in cells.[10]

In this work, using two particles held in optical traps to deform the RBC, the mean force and the particle fluctuations are measured. This allows us to explore a previously unchartered area of RBC mechanics in terms of the effects of pre-stress and the range of strain amplitude. Various protocols are compared: passive and active displacements; stress-strain *versus* stress relaxation experiments. We show clearly the onset of stiffening (*i.e.* non-linearity), already at very small strain. There is no evidence of non-thermal motion in the range of $1.6 < \omega$ (rad s^{-1}) < 32, within the precision of our data. The question of non-thermal activity at lower frequencies remains open.

2 Materials and methods

RBCs are obtained by drawing ~100 μl of blood from one healthy donor by a fingertip needle prick. The blood is diluted in phosphate-buffered saline (PBS) with acid citrate dextrose and 1 mg ml^{-1} bovine serum albumin (BSA) at pH7.4 (reagents all from Sigma-Aldrich). To isolate the RBCs, the suspension is washed three times by centrifugation. The final buffer consists of 1 mg ml^{-1} BSA in PBS solution. The optical tweezers setup consists of a laser ($\lambda = 1064$ nm, $P_{max} = 1.1$ W) focused through a water immersion objective (Zeiss, Achroplan IR 63x/0.90 W) trapping from below. Technical details have been reported previously.[7] In brief, the laser beam is steered *via* a pair of acousto-optic deflectors allowing multiple trap generation with sub nanometre position resolution. A new laser position can be updated every 50 μs. In this work the trapping stiffness on each of two beads is either kept very low at $k_{trap} = 3$ pN μm^{-1} for experiments in which beads are weakly trapped to enable measurement of fluctuations, or much higher at $k_{trap} = 44$pN μm^{-1} to enable the largest possible cell stretching. The video is recorded with a fast CMOS camera (Allied Vision Tech., Marlin F-131B) at up to 1 kHz frame rate and with 0.1 ms exposure time. Experiments are carried out in a temperature controlled room ($T \simeq 23$ °C) but the local temperature in the sample is $T \simeq 30$ °C as established by measuring the buffer viscosity through the Brownian motion of trapped beads, a local heating consistent with ref. 34.

Carboxylated silica beads of radius $R = 2.5$ μm (Bangs Labs) are functionalized for attachment to the RBC by coating with Lectin and EDC (Sigma), following Bangs Labs technote 205. Using the tweezers, two beads are attached uniaxially on the equatorial plane of an RBC, at opposite ends, see Fig. 1. The construct is then floated away from the bottom glass slide surface (up to about 10 times the bead diameter). In this way the hydrodynamic drag from the solid glass surface is minimal. The

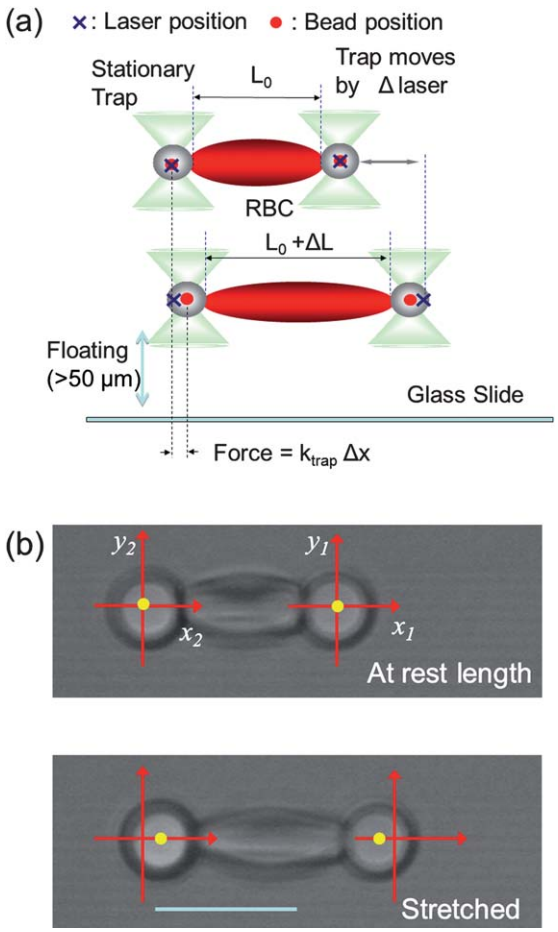

Fig. 1 Red blood cells can be stretched using optically trapped colloidal beads as handles. A schematic diagram of the stretching arrangement is shown in (a), where a cross marks the positions of the laser trap and a dot marks the center of the bead. The bead position is obtained *via* image analysis. The optical image is recorded onto a fast CMOS camera, typical snapshots with the RBC at rest and in a stretched state are shown in (b), where the beads are 5 μm in diameter. Fluctuations of each bead are labeled as (x_i,y_i) with $i = 1,2$, and are measured relative to the equilibrium position of the bead. For a cell held at its rest length, the bead equilibrium position corresponds to the laser trap position. Scale bar is 10 μm.

area of contact between the bead and the cell is estimated to be in the range 3–4.5 μm² from the microscopy images, and no significant correlation of the patch area with any of the experimental results was observed. The cells are quite monodisperse in size, with an initial cell length (the diameter) $L_0 \simeq 8\mu$m. This is the experimental arrangement first demonstrated in the work of ref. 35.

The coordinates in the image plane of the two beads are extracted *via* correlation filtering and a two-dimensional fitting, and are precise to a resolution of around 5 nm. The displacement of bead i from its average position (in fluctuation experiments) is labeled as $(x_i(t),y_i(t))$, with $i = 1,2$.

Three deformation protocols are explored in this work and described below: measurement of membrane mechanics from fluctuations; stiffness of the cell from stress *versus* strain data, and the time-dependent stiffness measured in stress relaxation. Greater detail is given on the fluctuation experiment, as the other methods have been reported before.[7]

2.1 Fluctuations

2.1.1 Power spectra. The fluctuations of the trapped beads attached to the red blood cell are measured *via* image analysis. Bead motion can originate from either thermal noise alone, or from a combination of thermal and active processes in the cell: this is an open question. Fluctuations are recorded for the cell at rest length L_0 (un-stretched) and at two increasing degrees of stretching. These fluctuations are analyzed *via* the framework of microrheology,[29,10] to extract the cell stiffness (elastic and dissipative components).

The bead positions are recorded for 1 min. We focus here on the dynamics in the axial x-direction, and calculate various functions: the autocorrelation of each bead in time $C_i(t') = \langle x_i(t)x_i(t+t')\rangle_t$, the autocorrelation of the relative fluctuations between beads (these are the fluctuations of cell length) $C_\delta(t') = \langle (x_2(t) - x_1(t))(x_2(t-t') - x_1(t-t'))\rangle_t$, the crosscorrelation function $C_{ij}(t') = \langle x_i(t)x_j(t+t')\rangle_t$, $(i \neq j)$. To simplify notation, $\delta x(t)$ will be used for $x_2(t) - x_1(t)$. From these functions, the power spectra are obtained *via* a Fourier transform:

$$\begin{aligned} P_{x_i}(\omega) &= F.T.[C_i(t')], \\ P_{\delta x}(\omega) &= F.T.[C_\delta(t')], \\ P_{cross}(\omega) &= F.T.\left[C_{ij}(t')\right], (i \neq j). \end{aligned} \tag{1}$$

In Fig. 2, spectra of $P_{\delta x}(\omega)$ are shown for different experimental conditions. The data is taken from a video at frame rate 470 Hz, and is 63 s long. The lowest angular frequency in the dataset is 0.1 rad s^{-1} and the Nyquist frequency is 1500 rad s^{-1}. Data is shown from one decade above the minimum (so that some averaging is possible to reduce noise) up to 2/3 of the Nyquist frequency. The fitting range 70 to 700 (rad s^{-1}) in the spectrum has been chosen to start from after the roll-off in the spectrum, and terminate at half the Nyquist frequency.

The autocorrelation function of the displacements of a single thermally excited bead trapped in a harmonic potential with stiffness k_{trap} (in the absence of a cell or other beads) is an exponential decay with timescale $\tau = \gamma_{drag}/k_{trap}$, where $\gamma_{drag} = 6\pi\eta R$ is the hydrodynamic drag coefficient of the bead, in a solvent of viscosity η. Then the power spectrum is well known to be the Lorentzian:

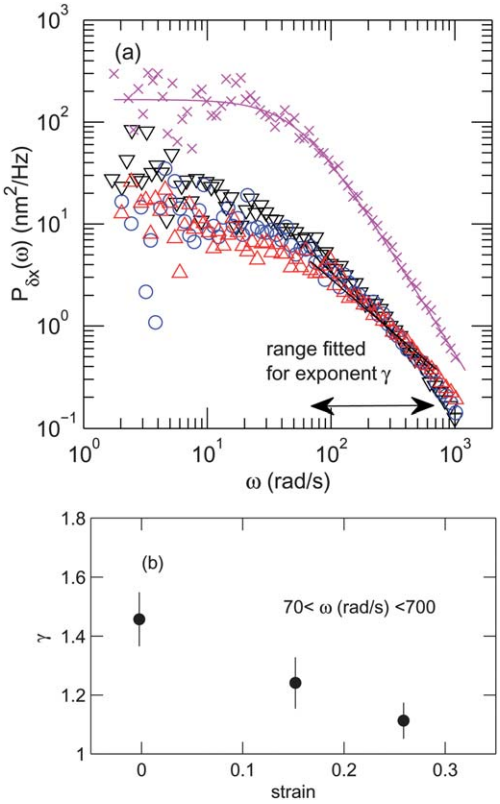

Fig. 2 (a) Power spectral density of the fluctuations of the inter-bead distance δx. Different states of strain lead to a change of the amplitude and shape of the spectrum: (▽) cell at rest, (○) and (△) are the cell stretched by 15% and 25% respectively. The spectra are fitted to a power law in the frequency range indicated, to obtain the exponent γ. The power law exponents for these spectra and those of all measured cells are plotted in panel (b). The (×) indicate the spectrum of δx for a pair of 5 μm diameter beads at the same distance (13 μm center to center) and optical trap conditions as in the cell stretching experiments. These data are fit with a generalized Lorentzian function in which the power of the high frequency regime is free to fit. The value of 2 is obtained as expected. The bandwidth of 1 Hz is used for the power spectral density as it is the common unit for this quantity, but note that the spectrum is plotted as a function of the angular frequency ω used throughout this paper. (b) The effect of strain on the power law exponents γ, for experiments at different states of cell strain. The value of γ decreases with strain: there are various interpretations of this as discussed in the text.

$$P_{x_i}(\omega) = \frac{2k_BT}{\gamma_{drag}(\omega_c^2 + \omega^2)}, \tag{2}$$

where ω_c is known as the corner (angular) frequency and is related to the stiffness and friction: $\omega_c = k_{trap}/\gamma_{drag}$. k_B is the Boltzmann constant and T is the absolute temperature. The square decay of the spectrum for high frequency is characteristic of dissipation in a Newtonian medium. With two beads at a distance d from each other in a liquid, there are hydrodynamic interactions that decay as $1/d$, as first calculated by Oseen;[36] the spectrum of fluctuation of each bead is modified as shown by Meiners and Quake.[37] In this scenario, the normal modes of the 2-bead system are the relative and the average motions. A simple Lorentzian form describes in particular the power spectrum for relative motion, $P_{\delta x}(\omega)$. This has the form of eqn (2) but the

corner frequency is reduced to $\tilde{\omega}_c = \omega_c 3R/(2d)$, reflecting the increased drag arising from interactions.

In the presence of a cell held between the beads, there is potentially a stronger coupling between the beads, and it may have an elastic as well as a viscous character. If the cell does not occupy a major fraction of the space between the beads, then also some hydrodynamic coupling through the surrounding fluid can still be felt. Because of the heterogeneous geometry around the bead, this scenario is more complex compared to standard microrheology where beads are embedded in a homogeneous material.[38] In the homogeneous case, it is possible to rigorously determine the material elastic shear properties, extending the Oseen interaction term to account for viscoelasticity.[38] Then, in case of externally trapped particles, it is also possible to take into account the contribution to fluctuations from the optical trap potential, and recover the material properties.[39] For the more complex (heterogeneous) system in which a cell is present in-between the two beads, it is necessary to make approximations. The way we have proceeded is to use the formalism of ref. 39 to calculate the system susceptibility, to remove the contribution of the trap potentials, and to obtain an effective stiffness that describes the interaction between the beads. This stiffness will contain the whole interaction, through the cell and the surrounding liquid.

The spectrum $P_{\delta x}(\omega)$ can be expected to remain frequency independent for low enough frequencies, and to crossover to a ω^{-2} decay at sufficiently high frequencies. However in the intermediate frequency range, the spectrum can exhibit in principle any intermediate decay rate, reflecting the existence of additional dissipative processes. Finally, the amplitude of $P_{\delta x}(0)$ in the presence of a cell need not remain the same as without the cell, since the cell itself can contribute a zero-frequency finite elastic response component.

Systematic effects due to the camera exposure (*i.e.* integration) time and finite frame rate have to be considered. For spectra that decay with a single power of the frequency, $P \sim \omega^{-\gamma}$ for $\omega \gg \omega_c$, these factors can be addressed by the technique explained in ref. 40, allowing an analysis up to frequencies close to the Nyquist limit ω_{Ny}. Having considered these effects, it was concluded that with the experimental parameters in this work there is no observable contribution from this effect to the data below $\omega_{Ny}/2$, and only this data was used. Calibration data in the absence of a cell show in Fig. 2 a good agreement to a generalized-Lorentzian spectrum where the decay exponent γ is a free parameter, obtaining $\gamma = +2.00 \pm 0.02$ consistent with the Lorentzian form of eqn (2).

2.1.2 Obtaining cell stiffness from the power spectra. The method follows closely ref. 39, except for the last steps where the stiffness is considered here rather than the shear modulus. Briefly, the susceptibilities for single and cross-correlated fluctuations are calculated *via*:

$$\begin{aligned} \chi''_{x_i}(\omega) &= \frac{\omega}{2k_B T} P_{x_i}(\omega) \\ \chi''_{cross}(\omega) &= \frac{\omega}{2k_B T} P_{cross}(\omega), \end{aligned} \tag{3}$$

which are expressions of the fluctuation-dissipation theorem. Then the real part of the susceptibility for single and cross cases is obtained through a Kramers–Kronig integral:

$$\chi'(\omega) = \frac{2}{\pi} \mathrm{P} \int_0^\infty \frac{\zeta}{\zeta^2 - \omega^2} \chi''(\zeta) d\zeta. \tag{4}$$

Physically, this is a consequence of causality. In ref. 39 it is shown how to compute this principal value integral *via* sine and cosine transforms (the real data is discrete, so these integral transforms are in practice discrete series), whereas we found it more convenient to use the Hilbert transform which is a pre-coded function in Matlab. Taking the Hilbert transform of an antisymmetric function built by "folding" $\chi''(\omega)$, and then taking one branch of the real component, gives $\chi'(\omega)$ equivalently to the integral of eqn (4). These susceptibilities contain not just the response of the beads to the cell+liquid system, but also still include the trapping potential.

Again following ref. 39, the trap effects can be removed to obtain the susceptibility for inter-particle response due purely to the cell+liquid system:

$$\alpha^*_{cross}(\omega) = \frac{\chi^*_{cross}}{1 - k_{trap}\chi^*_{x_1} - k_{trap}\chi^*_{x_2} - k^2_{trap}{\chi^*_{cross}}^2 + k^2_{trap}\chi^*_{x_1}\chi^*_{x_2}}. \tag{5}$$

Here the $\chi^* = \chi' + \chi''$ are complex quantities. This step simply requires the assumption of force/displacement linearity, which is expected to be valid for spontaneous fluctuations. The effective stiffness of the system can be defined as:

$$K^*(\omega) = \frac{1}{\alpha^*_{cross}(\omega)}. \tag{6}$$

For completeness, we remind the reader that if the material were homogeneous then the shear modulus could be derived from:

$$G^*(\omega) = \frac{1}{4\pi d \alpha^*_{cross}(\omega)}. \tag{7}$$

The procedure outlined here has been verified on data of pairs of colloids in water, with $R = 2.5$ μm and center-to-center distances of $d = 13$ μm as in the RBC experiments, and also with numerically generated data exploring parameter space (including hydrodynamic interaction *via* the method of Ermac and McCammon,[41] as in ref. 42). Treating this data, for which all the functions ($C(t)$, $P(\omega)$, $\chi(\omega)$, $\alpha(\omega)$, $G(\omega)$) are known analytically,[37] allows one to verify separately the effects of finite frame rate and finite experiment length, which introduce artifacts at high and low frequency respectively. The results are reported here for $K^*(\omega)$ in the frequency range where these effects can be neglected.

2.2 Stress relaxation

One laser is displaced rapidly to a new position; the cell is therefore also stretched rapidly. The force right after the displacement is higher than the equilibrium value, and the force relaxation is measured as a function of time. Different amplitudes of strain are tested. The case in which the cells are initially at rest length is compared to a pre-stretched condition.

2.3 Stress *versus* strain

Moving the beads with the optical traps, the force on the bead is measured *versus* cell elongation. This is done for small-amplitude strains starting with the cell at the rest length L_0, and for small

amplitude strains on top of a pre-stress (obtaining a "differential modulus" as in ref. 22). Different pulling rates are explored, and a comparison is also made with larger amplitude deformation. The force *versus* the cell elongation data is fit to a linear function, the gradient of which is the cell stiffness K.

3 Results and discussion

3.1 Fluctuations

3.1.1 Passive spectrum. Previous experiments[27,28] have considered the motion of a single bead attached to an actin-filament coated vesicle. The current setup is similar, with the cell being held by "soft" potentials on either side. If the trapping potentials are equal, looking at the spectrum of a single bead is not ideal: the normal modes are given by the difference and the average of the bead positions. We focus first on $P_{\delta x}(\omega)$ for comparison to ref. 27,28. The membrane exerts a force on the attached beads, modifying the power exponent γ to a value less than 2. This can arise from both a bending energy and the in-plane viscoelasticity of the cell membrane.

The power exponent γ is obtained by fitting the $70 < \omega$ (rad s^{-1}) < 700 region of the power spectrum of $P_{\delta x}(\omega)$, as shown in Fig. 2. The average over all 15 independently measured cells is reported in Fig. 2(b), for cells at rest and stretched to various degree. The value of γ falls from 1.46 ± 0.09 at rest to 1.24 ± 0.09 at 15% strain, and 1.11 ± 0.06 at 25% strain. At much larger frequencies than can be measured with the current setup, a transition would be expected to a regime of ω^{-2} decay.[29] The root mean square displacement (rms) for the δx of beads trapped in water is 80.7 nm, and the rms of δx for beads attached to a cell is 48.8 nm, 45.9 nm and 45.3 nm as the cell is elongated (these are the values corresponding to the data in Fig. 2).

Membrane mechanics has been developed successfully starting from the free energy framework set out by Helfrich.[43] A similar theoretical analysis has been applied to experiments on vesicles[44,45] and on RBC.[25,46–48] Hydrodynamical aspects have been considered for the case of an RBC by Brochard and Lennon,[49] Peterson[50] and more recently by Safran and Gov.[51] The RBC out of plane membrane fluctuations have previously been modelled by two alternative approximations to the red blood cell shape; either as a sphere,[8] or as large planar membranes separated by a small gap.[52] In the high wavenumber limit, the spherical model can be approximated as the fluctuations of an isolated planar membrane. For this case, the membrane surface fluctuations can be expressed in a particularly simple form:[43]

$$\left\langle h_{\vec{q}}^2 \right\rangle = \frac{1}{A} \frac{k_B T}{\sigma q^2 + \kappa q^4}, \tag{8}$$

where the function $h_q(t)$ is the Fourier transform of the fluctuation amplitude $h(x,y)$, defined as:

$$h_{\vec{q}} = \frac{1}{A} \int_A h(x,y) \exp(-i\vec{q}\vec{x}) dx dy. \tag{9}$$

Here the wave vector $\vec{q}$ is two-dimensional, and its modulus q is given by $q^2 = q_x^2 + q_y^2$, σ is the tension on the membrane and κ is the bending modulus. To simplify notation, the vector sign in $h_{\vec{q}}$ will be dropped in the following. A shear modulus or a confining potential would appear as a q-independent term in the denominator of eqn (8), but it is clear experimentally that for an RBC this does not influence the observable fluctuation modes.[48] These membrane fluctuation modes are also hydrodynamic modes, and thus each mode has a single well defined relaxation timescale and a corresponding crossover frequency ω_q in a Lorentzian spectrum.[28] The power spectrum of displacements of one point on the membrane is given by a sum over all the dynamics at that point:

$$\left\langle \delta h^2(\omega) \right\rangle = 2 \sum_q \left\langle h_q^2 \right\rangle \frac{\omega_q}{\omega_q^2 + \omega^2}. \tag{10}$$

The quantity $\langle \delta h^2(\omega) \rangle$ is comparable, within factors of order unity, to the power spectrum of bead fluctuations $P_{\delta x}(\omega)$ described before. In what follows, we maintain the notation $\langle \delta h^2(\omega) \rangle$ for the theoretical calculations of the membrane point-displacement, and we focus on the dependence on ω of this quantity. The sum of eqn (10) can be approximated by an integral, and then calculated analytically in the limit cases that either tension σ or bending modulus κ dominate the fluctuation spectrum of eqn (8). In these cases ω_q is a simple function. The asymptotic behavior for the power spectrum for out-of-plane height fluctuation on the membrane can be calculated as in (28) if the tension is negligible, where $\omega_q = \kappa q^3/(4\eta)$:

$$\left\langle \delta h^2(\omega) \right\rangle \propto \kappa^{-1/3} \omega^{-5/3} \text{ (for } \sigma \simeq 0), \tag{11}$$

And an analogous calculation in the opposite limit of large tension, where $\omega_q = \sigma q/(4\eta)$ gives:

$$\left\langle \delta h^2(\omega) \right\rangle \propto \sigma^{-1} \omega^{-1} \text{(for } \kappa \simeq 0). \tag{12}$$

For high frequencies, and high wavenumber, the alternative model of two planar membranes has the same behaviour as the free membrane model above. This is because the distance over which the hydrodynamic interaction acts decays with increasing wavenumber. However, as discussed in,[52] at intermediate frequencies and wavevectors there is another set of modes, called the peristaltic modes, for which the opposite faces of the RBC are coupled hydrodynamically. These modes are relevant for RBCs since the RBC thickness in the centre of the cell is comparable to the wavelength of fluctuations which relax on typical experimental timescales. The power spectrum of the peristaltic fluctuations is calculated in ref. 52, and the limit cases are:

$$\left\langle \delta h^2(\omega) \right\rangle \propto \kappa^{-2/3} \omega^{-4/3} \text{(for } \sigma \simeq 0), \tag{13}$$

and:

$$\left\langle \delta h^2(\omega) \right\rangle \propto \sigma^{-1} \omega^{-1} \text{(for } \kappa \simeq 0). \tag{14}$$

In ref. 51, identical behaviour is obtained, but the calculation is there based upon the interaction between the membrane and the cytoskeleton, rather than between two membranes. In experiments on free red blood cells, where tension can normally be neglected, power spectra with exponents of $-4/3$[52,51] (analysing data from ref. 53), and $-5/3$[8] have both been observed. In (8), the flickering was observed up to kHz frequencies, whereas ref. 51,52 were limited by a maximum frequency of less than 100 Hz, so it is not surprising that different behaviour has been observed. Another difference lies in the geometry of the experiments. In ref. 8, observations were made of the flickering of the RBC equator,

whereas ref. 52 focused on the height difference of the two membranes, and ref. 51 on the absolute height of one membrane above a surface. It remains unclear what behaviour one would expect for the fluctuations of an RBC equator, when the flat region at the centre is in the peristaltic regime, since this situation is not described well by either approximation to the RBC shape. For the model of membrane-cytoskeleton interactions,[51] the power spectrum on the equator should be similar to that in the centre of the cell, whereas for the membrane-membrane interaction model,[52] the equator could be in a free membrane regime while the centre of the cell is undergoing peristaltic fluctuations. The shape of the RBC is such that the equator is much further away from contact with other parts of the membrane, compared to membrane near the centre of the cell. In either case, one can suppose that in the tensionless limit, the power spectrum of fluctuations on the equator lies between −4/3 and −5/3. However, ref. 25 has measured exponents as low as −0.9 for the contour fluctuations of free RBCs in isotonic media.

3.1.2 Effect of membrane constraints. Further complications arise when the RBC is connected to a perturbing force sensor, such as beads in optical traps. This has two effects upon the power spectrum. Firstly, the trap stiffness and the viscous drag on the bead must both be included in the total stiffness of the system, and secondly, the finite bead size prevents the high wavevector fluctuations of the membrane to translate into bead motion. The first effect is best seen by first calculating the susceptibility of the free membrane, in the planar approximation. This can be done following ref. 29,54:

$$\chi_{\text{membrane}} = \frac{1}{A}\sum_q \frac{\omega_q + i\omega}{4\eta q(\omega_q^2 + \omega^2)}. \quad (15)$$

In the limit where tension dominates, the real part of the susceptibility diverges. What this means, physically, is that, in the limit of zero curvature energy, an infinitely thin tether can be pulled out with zero additional area, and at no extra energy cost. From eqn (3), the real part of the susceptibility would not affect the power spectrum of a free RBC. However, in the same limit, the RBC stiffness vanishes, so that, when attached to trapped beads, the stiffness of the system, and therefore, the power spectrum, is entirely dominated by the trap stiffness and the viscous response of the beads. The only effect of the membrane is its purely hydrodynamic interaction with the beads, which an effect not modelled here. The same divergence occurs when tension dominates in the peristaltic models of ref. 52 and ref. 51. It is a general effect whenever the exponent in the power spectrum approaches −1, for related models including confinement terms due to the cytoskeleton, or the membrane viscosity. However, the limit of $q_{max} \to \infty$ is unphysical. Even for a free membrane, the fluctuations are cut off at the molecular length-scale. For an attached membrane there is an earlier cutoff in observable fluctuations, at the finite size of the bead attachment. In ref. 29 a sharp cut off in wavenumber is imposed at the bead radius. A refinement of that idea is to model the finite contact by modifying the susceptibility in eqn (15) to:

$$\chi_{\text{membrane+patch}} = \frac{1}{A}\sum_q \frac{f(q)(\omega_q + i\omega)}{4\eta q(\omega_q^2 + \omega^2)}, \quad (16)$$

where $f(q) \approx \frac{2\pi}{\rho q}$, for $q > \frac{2\pi}{\rho}$, and $f(q) = 1$ otherwise. This expression is comparable to the susceptibility from bead fluctuations, obtained in eqn (3) and 4, except that the bead hydrodynamic interaction with the solvent and with the other bead is not included in eqn (16). To justify eqn (16) briefly, the contact between the bead and the membrane is modelled as a ring of radius ρ. The Fourier transform of this ring contact is a Bessel function of the first kind, which decays as a sinusoid multiplied by $q^{-1/2}$. The square of this Fourier transform gives the multiplicative factor $f(q) \approx q^{-1}$. The crossover frequency is the same as that described for the sharp cutoff in ref. 29, but the additional factor of q^{-1} which arises here modifies the high frequency limit of the single planar membrane power spectrum in both high tension and low tension limits to:

$$\delta h^2(\omega) \propto \omega^{-2} \text{ (for high frequency, with patch, planar case)}, \quad (17)$$

recovering the scaling of Stokes damping of a bead in a trap. Note however that the bead itself is not present in this model (*i.e.* there is no bead drag) and therefore the prefactor of this spectrum is not comparable quantitatively to the experiment. In ref. 28 the crossover effect was measured experimentally as a function of bead size. Therefore, the exponents given in eqn (11) and (12) are transient regimes which decay into the unbound bead power spectrum. Because of the vanishing of the membrane stiffness noted earlier, in the limit of low κ, the ω^{-1} regime is found to be extremely short lived (less than one decade in frequency), over a realistic range of patch sizes and membrane parameters ($\sigma < 10^{-2}$ N m^{-1}, $\kappa < 10^{-17}$ J, $\eta_{int} < 0.4$ Pa s, $\rho < 3$ μm), when the power spectrum is calculated for a spherical membrane including bead interactions. However, in the case of the peristaltic model, performing the same analysis, and naively including the multiplicative factor $f(q)$ for the finite bead radius in the relevant integrals for the power spectra found in ref. 52, gives modified exponents:

$$\langle \delta h^2(\omega) \rangle \propto \kappa^{-1/2}\omega^{-3/2}$$

$$\text{(for } \sigma \simeq 0\text{, with patch, peristaltic modes)}, \quad (18)$$

and:

$$\langle \delta h^2(\omega) \rangle \propto \sigma^{-3/4}\omega^{-5/4}$$

$$\text{(for } \kappa \simeq 0\text{, with patch, peristaltic modes)}, \quad (19)$$

which can persist for longer than the current experimental frequency range. These exponents agree with the exponents found here for the unstretched and slightly stretched RBC power spectra, where one would expect a cross-over from a bending dominated to a tension dominated regime. However, the naive translation of the peristaltic modes into fluctuation amplitudes on the RBC equator, is not well justified, while the rigorous calculation of power spectra for a real RBC shaped membrane has not yet been achieved.

The interpretation of the exponent γ may be furthermore complicated by the possibility that, as in actin coated membranes, the protein filament network of the RBC could play a mechanical role, introducing another source of frequency dependence.[29] In this case, calculating a value of γ becomes very difficult. Complex protein networks may even contribute non-thermal noise, if there are ATP-fueled rupture events.[8] This latter

possibility is explored here below, by comparing the cell response measured from intrinsic motion and to that from active deformation.

3.1.3 Stiffness of the cell from fluctuations. The stiffness obtained from analysis of intrinsic motion is plotted in Fig. 3. The real component $K'(\omega)$ is practically frequency independent, whereas the imaginary component $K''(\omega)$ scales linearly with ω. Following this observation, the real part has been fitted to measure the constant value of K', which is reported in Fig. 6 for comparison with active stiffness measured as a function of frequency.

The dissipative component of the stiffness, fitted linearly, gives a value consistent with the dissipation from hydrodynamic drag of two beads at the experimental center-to-center distance, in a liquid of viscosity slightly larger than water. It is difficult to discuss this result more quantitatively because the hydrodynamic interaction in the presence of the cell is not modeled simply. An interesting observation is that the dissipation is small; this is in contrast to the large dissipation observed for active and big elongations in our previous work,[7] reinforcing the conclusion that additional dissipative processes are at work when the cell is deformed actively. These are processes (*e.g.* stress-induced rupture or protein un-folding) which do not contribute to the spontaneous motion of the membrane.

3.2 Relaxation

Stress-relaxation experiments are performed by displacing just one bead by rapidly moving one laser trap (within 50 μs) to a position between 0.5 μm and 2.0 μm from the rest position. This corresponds to straining the cell by a Δstrain jump in the range 0.04 to 0.14. A larger displacement is also explored (Δstrain = 0.25, moving the laser trap by 3.5 μm), but with a slower jump (time to move laser trap of 20 ms). The stress relaxation is measured starting from an appropriate first time-point, to reflect the time taken in straining the cell, as shown in the data of Fig. 4. The stress relaxation is recorded for 30 s at ~240 frames/s. Then the traps are returned to the rest position, and the same cell is stretched again after waiting typically 10 s. A typical experiment trace is shown in Fig. 4 (b).

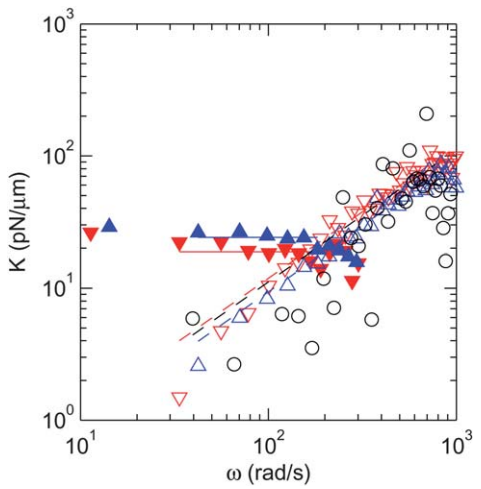

Fig. 3 Extracting the system susceptibility from thermal fluctuation, and using the Kramers–Kronig relation as shown in the text, it is possible to extract the complex stiffness as a function of frequency: $K^*(\omega)$. The data show an elastic stiffness for $\omega < 100$ rad s^{-1}, and a predominantly dissipative stiffness for higher frequencies. Markers correspond to a cell at rest (▼) and at maximum strain 0.26 (▲). As usual, solid markers indicate the real component, and open markers the imaginary component. The "apparent" stiffness due to water is shown by (○): it is exclusively dissipative, and arises from the hydrodynamic interaction of the two colloidal particles.

As in previous work[7] the time-dependent stiffness of the RBC is defined as $K(t) = F(t)/(L_0 + \Delta L(t))$. The total set of experiments is fitted very well by the following 3-parameter power-law function:

$$K(t) = K_\infty + \Delta K(t) = K_\infty + \Delta K_0 (t/t_0)^{-\alpha}, \qquad (20)$$

where $t_0 = 1s$ is fixed for a dimensionless time. The relaxation experiments have been carried out on 8 different cells, and the time dependent component $\Delta K(t)$ is plotted in Fig. 4 (a). The success of eqn (20) highlights that the time-dependent component of the stiffness decays as a power law. Within the experimental resolution, a plateau value is reached in around 30 s.

To study the effect of prestress, cells are stretched to $\Delta\text{strain}_{prestress} = 0.125$. After waiting 30 s a further rapid strain is applied, and stress-relaxation is observed as described above. The same cell is stretched repeatedly, as illustrated in Fig. 4 (b).

Changing the amplitude of the step strain when straining from the rest position does not affect the exponent α of the power-law relaxation. Values are between $0.50 < \alpha < 0.63$. However, the stress-relaxation from a prestress condition leads to a slightly lower exponent $0.38 < \alpha < 0.42$. Without prestress, the power law exponent values are quite similar to previous work where, under slightly lager strains, values of $\alpha = 0.75$ were measured for fresh cells, and $\alpha = 0.82$ measured for cells aged 1 day in glucose-starved conditions.[7] The value of 0.64 was measured by another group.[55]

Cell cytoskeletal networks are well known to be highly nonlinear, with an elastic modulus that depends sensitively on applied stress.[2] The experiments on the RBC show that a relaxation from small strain is similar to that obtained in the largest strain currently accessible with our system. The lower exponent value in the prestressed state could be evidence that prestress induces a change in the cell structure, a kinematic hardening. The kinematic hardening may result from a rearrangement of the spectrin network, by local restructuring through breaking and reforming the mesh structure of the spectrin network.[56] In previous work[7] by comparing the stress relaxation with stress-strain measurements and by measuring the energy dissipated on deformation, we also concluded that deformation was causing a structural change in the cell.

3.3 Stress–strain measurements

The modulus of the cell can be obtained from measuring the force necessary to pull the cell, as a function of the strain. In the absence of dissipation (*e.g.* for a very slow deformation) the gradient of the force *versus* strain data is the elastic component of the cell stiffness. For finite deformation rates, it is more significant to perform an oscillatory strain, and to obtain the in-phase

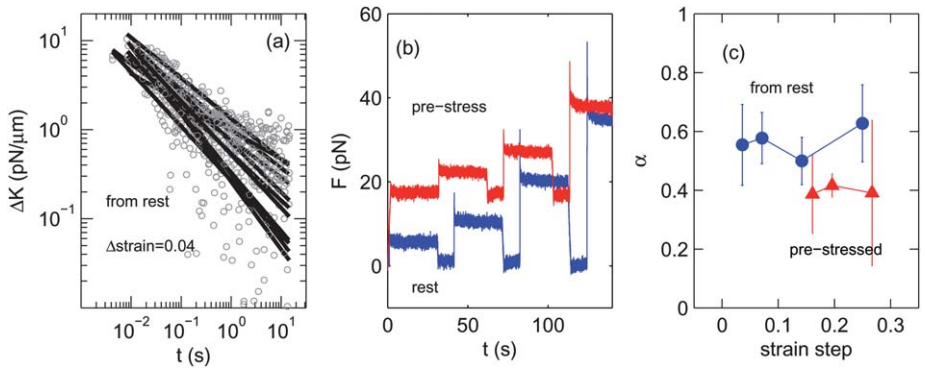

Fig. 4 The decay of the measured time-dependent part of the cell stiffness $\kappa(t)$ as a function of time can be fit with a power law, obtaining the exponent α. Panel (a) shows the data traces for a number of cells. The solid lines are power-law fits to individual experiments, showing the degree of noise characteristic of these experiments. (b) Typical time-course of an experiment run, showing force *versus* time. Two traces are shown, illustrating step strain from rest and from a pre-stressed condition. Force relaxation is measured for 30 s, with 10 s resting intervals. (c) The values of exponent α measured from this data, as a function of the strain step. The markers indicate (•) cells initially at the rest length and (▲) cells under pre-stress. The step strain amplitude does not change the value of the exponent α, but the prestress state is important, reducing the observed power exponent.

and out-of-phase components of the response, which are proportional to the elastic and dissipative components of the stiffness.[57] Small deformations (strain amplitude 0.02) are performed at initial strains of 0, 0.13 and 0.25, and large deformations (amplitude 0.13) are performed at initial strains of 0 and 0.13. Laser trap displacement speeds are 20, 5, 1 and 0.2 μm/s. Fig. 5, panels (a)∼(d) show the force *versus* applied strain, for different deformation speeds. With the smaller deformation compared to previous work,[7] the data have too much noise to back out both phase and amplitude. Therefore the force–strain data is fitted linearly, measuring the quantity $|K^*|$.

As the strain amplitude increases, the cell stiffness $|K^*|$ also increases, and begins to saturate at around strain 0.20. For the lower speeds of displacement, the stiffness at small amplitudes is smaller than the stiffness at large amplitudes. Stiffening with increasing deformation rate is very clear in Fig. 6, and extends the previous results of ref. 7 to a wide strain amplitude range. This is a simple but physiologically important aspect of RBC mechanics.

Considering in greater detail the stiffness dependence on amplitude and rate in Fig. 6, it can be seen that: (1) at rest length there is a stronger frequency dependence compared to pre-strained conditions; (2) pre-strain affects the lower frequencies more than the high frequency; (3) at the high frequencies, $\omega \gtrsim 10$ rad s^{-1}, $|K^*|$ is independent of deformation amplitude, whereas at low frequencies there is significant strain stiffening. These points are consistent with the rheological frequency-dependence obtained from fluctuations, shown in Fig. 3: At rest and at low pre-strain, the cell response is dominated by the elastic branch of K' at low frequencies, crossing over to a dissipative

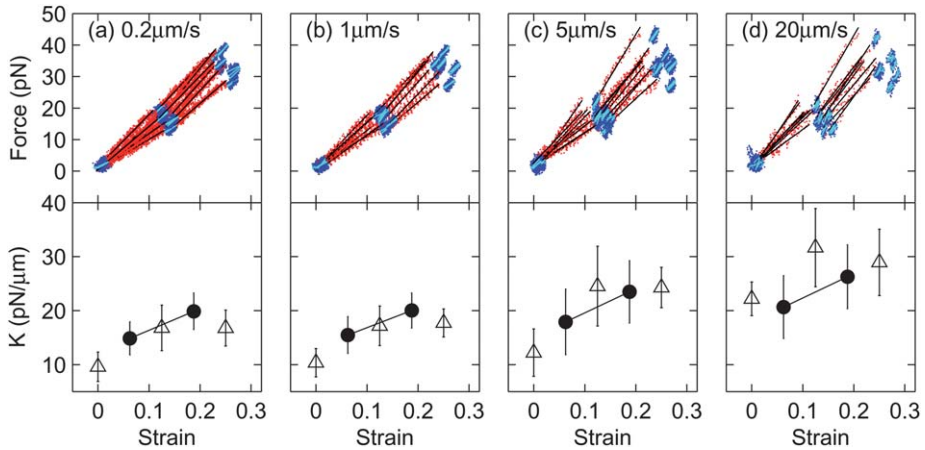

Fig. 5 The deformation speed has a strong effect on the measured cell stiffness. The measured stiffness also increases if the cell is pre-strained. The measured force (top) and stiffness (bottom) derived from it are plotted *versus* the strain of the cell, for different deformation speeds: (a) 0.2 μm s^{-1}, (b) 1 μm s^{-1}, (c) 5 μm s^{-1} and (d) 20 μm/s. The force *versus* strain data is fitted linearly (solid lines) to obtain $|K^*|$. Both small (blue markers) and large (red markers) strain amplitudes are explored: The symbols (•) indicate stiffness from large oscillations (around 0.13 strain amplitude; laser displacements of 1.75 μm), while (△) derive from small oscillations of around 2% amplitude (laser trap moves of 0.25 μm). Further measurements around the pre-strain of 0.13 have been done for two additional amplitudes: 4% and 7% (not shown in figure). All the stiffness values are plotted as a function of frequency in Fig. 6.

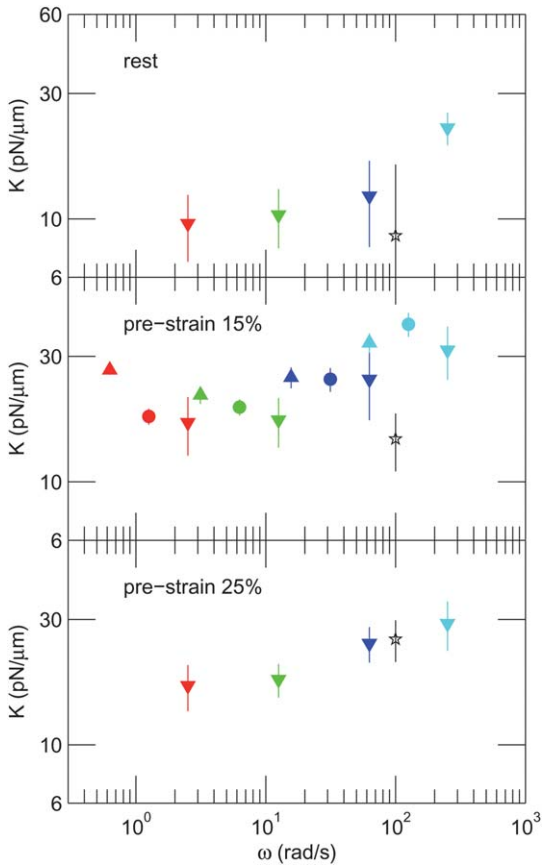

Fig. 6 The stiffness $|K^*|$ measured with active deformation shows a strong dependence on the strain of the cell and on the amplitude of deformation, and a weak trend with frequency. Different stiffness as the deformation amplitude is changed is a signature of non-linear elasticity. Different markers indicate the amplitude of driven deformations: (▲) is 7%, (●) is 4% and (▼) is 2%. While for a given strain amplitude there is only a very slight stiffening with frequency, there is a marked softening on reducing the amplitude of deformation. The (★) markers indicate the values of stiffness K' obtained by processing the fluctuation data as described in the text. These have been plotted at $\omega = 100$ rad s^{-1}, although as is shown in Fig. 3 this is a constant value in the range $20 < \omega$ (rad s^{-1}) < 200. The bead fluctuations can be considered as the smallest possible amplitude. The stiffness measured by fluctuation of the beads, for cells at rest or at small strain (15%), is smaller than that measured from actively driving cell oscillations. For large strains the two methods converge.

branch around $\omega \simeq 200$ rad s^{-1}; the K' value increases with cell strain, whereas the K'' remains the same. The data of Fig. 6 shows this behavior, with the increase of $|K^*|$ with ω for the cell at rest, and the increase of the low-ω range of $|K^*|$ as the cell is stretched. These results, separating out the effect of amplitude and deformation frequency, clearly characterize the nonlinearity of cell mechanical response.

The K' values obtained from fluctuations are plotted in Fig. 6 and show that for the cell at rest or pre-strained by 15% there is already a small difference between the infinitesimal strain motion, and the 2% oscillations. This small difference seems consistent with a "leveling-off" of K to a finite value at zero amplitude oscillation. In other words, there is no evidence in the data of Fig. 6 to suggest significant non-thermal sources of motion, which would result in an apparent K from fluctuations much smaller than the $|K^*|$ from active motion. This statement can only be made here for the frequency range $10 < \omega$ (rad s^{-1}) < 200 ($1.6 < f$ (Hz) < 32) probed in the fluctuation experiment. It leaves open the possibility of non-thermal sources at lower frequency: indeed Betz *et al.* [8] measured non-thermal motion in the range $0.1 < \omega$ (Hz) < 10, with the strongest non-thermal activity at 1Hz. It should be noted that the cells considered here gave rise to a spread of K' values at rest: In Fig. 6 the data from one cell at rest shows a $K' \simeq 20$ pN μm^{-1}, whereas of the 15 cells considered the average and standard deviation at rest are $K' \simeq (9 \pm 7)$pN μm^{-1}. This large spread appears due to differences between cells. This data is consistent with the absence of non-thermal noise, but the error bars are such that non-thermal noise cannot conclusively be ruled out.

The occurrence of non-linearity at such small strains, smaller than for *in vitro* reconstituted networks, may be a consequence of the state of tension in the spectrin network. We have previously put forward in ref. 7 the idea that the cytoskeleton non-linearity is a consequence of stress-induced rupturing or re-modeling of the network. This type of effect would give rise to mechanical behavior consistent with the soft glassy rheology (SGR) model. The SGR model is a conceptual model describing the response of material capable of flowing only under the action of external forces,[58] and has been applied successfully to cell mechanics[59] and *in vitro* reconstructed cytoskeleton models.[60] The success of the model appears linked to the fact that the components of the cytoskeleton responsible for the elasticity are mechanically fragile, a condition with strong analogies to a wormlike chain solution.[61] In the RBC, proteins that bind the spectrin filaments to the membrane are known to dissociate by consumption of ATP, allowing the cell to change shape: These are transient bonds, under physiological conditions.[62] It is therefore not unreasonable to assume that external stress facilitates this process of rupture of the most fragile bonds, with formation of new bonds; the newly formed bond would carry (on average) less force than before rupture. The fact that the cell has a long-time elastic modulus implies that only a fraction of the bonds can break. In this case a prestress leads to a state with residual stress, carried by the permanent bonds, with the transient bonds playing a negligible role. This is consistent with the observation that for a large pre-strain (of 25%) the difference of measured modulus with differential amplitude vanishes. This picture with two types of bond (transient and permanent) also explains why the RBC does not go into a "fluidised" low modulus state as in ref. 59 upon deformation. A simulation such as carried out in ref. 63, where rupture events are included, seems relevant and could be extended to include a fraction of permanent bonds.

4 Conclusions

In summary, we have studied the mechanical properties of red blood cells by monitoring the motion and forces acting on two optically trapped probe beads attached uni-axially. Different deformation protocols have been performed, aiming to elucidate the limit of linear response. Careful consideration has been given to the characteristics of the spontaneous fluctuations, comparing the power law seen in experiments with values calculated from the theory of membrane deformation. The exponent observed experimentally changes as the cell is stretched, consistent with the

idea of an increasing membrane tension. For the cell at equilibrium, there is evidence of hydrodynamic interactions between the opposite planes of the RBC. The experiments reported here also allow us to compare the response of the cell over a carefully controlled range of deformation amplitude. It has been shown that the cell stiffness changes already for very small strains, of the order of a few percent. Previous results in the literature had reported non-linearity, but only at larger strains where geometric effects would also be important.

Finally, the comparison of the intrinsic cell susceptibility with the response under external forces has indicated that non-thermal effects are not required to explain the results from these experiments. However given the experimental uncertainty non-thermal noise as in Betz *et al.* [8] cannot be ruled out. Future experiments should be aimed at extending these results to a lower frequency range and in reducing the experimental error, to confirm or exclude directly the presence of non-thermal effects.

Acknowledgements

We acknowledge useful discussions with Christoph Schmidt and Eugene Terentjev. This work was supported by the Korea Foundation for International Cooperation of Science & Technology (KICOS) through a grant provided by the Korean Ministry of Education Science & Technology (MEST) in 2009-00591.

References

1 B. Hoffman, G. Massiera, K. Van Citters and J. Crocker, *Proc. Natl. Acad. Sci. U. S. A.*, 2006, **103**, 10259–10264.
2 K. Kasza, A. C. Rowat, J. Liu, T. E. Angelini, C. P. Brangwynne, G. H. Koenderink and D. A. Weitz, *Curr. Opin. Cell Biol.*, 2007, **19**, 101–107.
3 B. Alberts, D. Bray, J. Lewis, M. Raff, K. Roberts and J. D. Watson, *Molecular Biology of the Cell*, Garland Publishing, New York, 2002.
4 D. A. Weitz and P. A. Janmey, *Proc. Natl. Acad. Sci. U. S. A.*, 2008, **105**, 1105–1106.
5 D. Discher, N. Mohandas and E. Evans, *Science*, 1994, **266**, 1032–1035.
6 T. W. Secomb, *Cell Biophys.*, 1991, **18**, 231–51.
7 Y. Z. Yoon, J. Kotar, G. Yoon and P. Cicuta, *Phys. Biol.*, 2008, **5**, 036007.
8 T. Betz, M. Lenz, J. Joanny and C. Sykes, *Proc. Natl. Acad. Sci. U. S. A.*, 2009, **106**, 15320–15325.
9 D. Boal, *Mechanics of the cell*, Cambridge University Press, U.K., 2002.
10 D. Mizuno, R. Bacabac, C. Tardin, D. Head and C. F. Schmidt, *Phys. Rev. Lett.*, 2009, **102**, 168102.
11 D. E. Discher, D. J. Mooney and P. W. Zandstra, *Science*, 2009, **324**, 1673–1677.
12 P. Moshayedi, L. da F Costa, A. Christ, S. P. Lacour, J. Fawcett, J. Guck and K. Franze, *J. Phys.: Condens. Matter*, 2010, **22**, 194114.
13 D. J. Montell, *Science*, 2008, **322**, 1502–1505.
14 X. Trepat, M. R. Wasserman, T. E. Angelini, E. Millet, D. A. Weitz, J. P. Butler and J. J. Fredberg, *Nat. Phys.*, 2009, **5**, 426–430.
15 B. Fabry, G. N. Maksym, J. P. Butler, M. Glogauer, D. Navajas and J. J. Fredberg, *Phys. Rev. Lett.*, 2001, **87**, 148102.
16 P. Pullarkat, P. Fernandez and A. Ott, *Phys. Rep.*, 2007, **449**, 29.
17 D. Mizuno, C. Tardin, C. F. Schmidt and F. C. MacKintosh, *Science*, 2007, **315**, 370–373.
18 G. H. Koenderink, Z. Dogic, F. Nakamura, P. M. Bendix, F. C. MacKintosh, J. H. Hartwig, T. P. Stossel and D. A. Weitz, *Proc. Natl. Acad. Sci. U. S. A.*, 2009, **106**, 15192–15197.
19 N. Wang, J. P. Butler and D. E. Ingber, *Science*, 1993, **260**, 1124.
20 N. Desprat, A. Richert, J. Simeon and A. Asnacios, *Biophys. J.*, 2005, **88**, 2224–2233.
21 P. Fernandez, P. A. Pullarkat and A. Ott, *Biophys. J.*, 2006, **90**, 3796–3805.
22 P. Fernandez and A. Ott, *Phys. Rev. Lett.*, 2008, **100**, 238102.
23 Y. Park, C. Best, K. Badizadegan, R. Dasari, M. Feld, T. Kuriabova, M. Henle, A. Levine and G. Popescu, *Proc. Natl. Acad. Sci. U. S. A.*, 2010, **107**, 6731–6736.
24 S. Tuvia, A. Almagor, A. Bitler, S. Levin, R. Korenstein and S. Yedgar, *Proc. Natl. Acad. Sci. USA.*, 1997, **94**, 5045–5049.
25 J. Evans, W. Gratzer, N. Mohandas, K. Parker and J. Sleep, *Biophys. J.*, 2008, **94**, 4134–44.
26 J. C.-M. Lee and D. E. Discher, *Biophys. J.*, 2001, **81**, 3178–3192.
27 E. Helfer, S. Harlepp, L. Bourdieu, J. Robert, F. Mackintosh and D. Chatenay, *Phys. Rev. Lett.*, 2001, **87**, 088103.
28 E. Helfer, S. Harlepp, L. Bourdieu, J. Robert, F. Mackintosh and D. Chatenay, *Phys. Rev. E: Stat. Phys., Plasmas, Fluids, Relat. Interdiscip. Top.*, 2001, **63**, 021904.
29 A. J. Levine and F. C. MacKintosh, *Phys. Rev. E: Stat. Phys., Plasmas, Fluids, Relat. Interdiscip. Top.*, 2002, **66**, 061606.
30 T. G. Mason and D. A. Weitz, *Phys. Rev. Lett.*, 1995, **74**, 1250–1253.
31 P. Cicuta and A. M. Donald, *Soft Matter*, 2007, **3**, 1449–1455.
32 P. Cicuta, S. L. Keller and S. L. Veatch, *J. Phys. Chem. B*, 2007, **111**, 3328–3331.
33 J. C. Crocker, M. T. Valentine, E. R. Weeks, T. Gisler, P. D. Kaplan, A. G. Yodth and D. A. Weitz, *Phys. Rev. Lett.*, 2000, **85**, 888–891.
34 E. J. G. Peterman, F. Gittes and C. F. Schmidt, *Biophys. J.*, 2003, **84**, 1308–1316.
35 S. Hénon, G. Lenormand, A. Richert and F. Gallet, *Biophys. J.*, 1999, **76**, 1145–1151.
36 J. Happel and H. Brenner, *Low Reynolds Number Hydrodynamics: with special applications to particulate media*, Kluwer, New York, 1983.
37 J. C. Meiners and S. R. Quake, *Phys. Rev. Lett.*, 1999, **82**, 2211–2214.
38 D. T. Chen, E. R. Weeks, J. C. Crocker, M. F. Islam, R. Verma, J. Gruber, A. J. Levine, T. C. Lubensky and A. G. Yodh, *Phys. Rev. Lett.*, 2003, **90**, 108301.
39 M. Atakhorrami, J. I. Sulkowska, K. M. Addas, G. H. Koenderink, J. X. Tang, A. J. Levine, F. C. MacKintosh and C. F. Schmidt, *Phys. Rev. E: Stat., Nonlinear, Soft Matter Phys.*, 2006, **73**, 061501.
40 W. P. Wong and K. Halvorsen, *Opt. Express*, 2006, **14**, 12517.
41 D. L. Ermak and J. A. McCammon, *J. Chem. Phys.*, 1978, **69**, 1352–1360.
42 J. Kotar, M. Leoni, B. Bassetti, M. Cosentino Lagomarsino and P. Cicuta, *Proc. Natl. Acad. Sci. U. S. A.*, 2010, **107**, 7669–7673.
43 W. Helfrich and R. M. Servuss, *Nuovo Cimento D*, 1984, **3**, 137–151.
44 H. G. Pecreaux, J. Dobereiner, J. Prost, J. F. Joanny and P. Bassereau, *Eur. Phys. J. E*, 2004, **13**, 277–290.
45 Y. Z. Yoon, J. P. Hale, P. G. Petrov and P. Cicuta, *J. Phys.: Condens. Matter*, 2010, **22**, 062101.
46 K. Fricke and E. Sackmann, *Biochim. Biophys. Acta, Mol. Cell Res.*, 1984, **803**, 145–152.
47 M. A. Peterson, H. Strey and E. Sackmann, *J. Phys. II*, 1992, **2**, 1273–1285.
48 Y. Z. Yoon, H. Hong, A. Brown, D. C. Kim, D. J. Kang, V. Lew and P. Cicuta, *Biophys. J.*, 2009, **97**, 1606–1615.
49 F. Brochard and J. F. Lennon, *J. Phys.*, 1975, **36**, 1035–1047.
50 M. A. Peterson, *Mol. Cryst. Liq. Cryst.*, 1985, **127**, 257.
51 N. Gov, A. G. Zilman and S. Safran, *Phys. Rev. Lett.*, 2003, **90**, 228101.
52 F. Brochard and J. F. Lennon, *J. Phys.*, 1975, **36**, 1035–1047.
53 A. Zilker, H. Engelhardt and E. Sackmann, *J. Phys. (Paris)*, 1987, **48**, 2139.
54 Note that eqn (15) is derived in the same way as eqn 39 of ref. 29, but includes membrane tension and does not include a cut-off wavevector.
55 M. Puig-de Morales-Marinkovic, K. T. Turner, J. P. Butler, J. J. Fredberg and S. Suresh, *Am. J. Physiol.: Cell Physiol.*, 2007, **293**, 597–605.
56 N. S. Gov, *Phys. Rev. E: Stat., Nonlinear, Soft Matter Phys.*, 2007, **75**, 011921.
57 R. G. Larson, *The Structure and Rheology of Complex Fluids*, Oxford Univ. Press, New York, 1999.
58 P. Sollich, F. Lequeux, P. Hebraud and M. E. Cates, *Phys. Rev. Lett.*, 1997, **78**, 2020.
59 X. Trepat, L. Deng, S. An, D. Navajas, D. Tschumperlin, W. Gerthoffer, J. Butler and J. Fredberg, *Nature*, 2007, **447**, 592.
60 C. Semmrich, T. Storz, J. Glaser, R. Merkel, A. R. Bausch and K. Kroy, *Proc. Natl. Acad. Sci. U. S. A.*, 2007, **104**, 20199–20203.
61 K. Kroy, *Soft Matter*, 2008, **4**, 2323–2330.
62 N. S. Gov and S. A. Safran, *Biophys. J.*, 2005, **88**, 1859–1874.
63 B. Hoffman, G. Massiera and J. Crocker, *Phys. Rev. E: Stat., Nonlinear, Soft Matter Phys.*, 2007, **76**, 051906.